The effect of CO_2 phase on drainage process by analysis of transient differential pressure

Xiaoqiang Jin [a], Cong Chao [a], Kejian Wu [b], Changyou Xia [c], Xianfeng Fan [a,*]

a Institute for Materials and Processes, School of Engineering, The University of Edinburgh, Edinburgh, EH9 3JL, UK

b School of Engineering, University of Aberdeen, Aberdeen, AB24 3UE, UK

c Shenzhen Research Center on Climate Change, School of Economics and Management, Harbin Institute of Technology (Shenzhen), Shenzhen, 518055, China

*Corresponding author: x.fan@ed.ac.uk

Abstract

CO_2 sequestrated in deep geological formations can be in gaseous, supercritical or liquid state, depending on subsurface pressure and temperature. In this work, CO_2 core flooding experiments are carried to investigate the effect of CO_2 phase on drainage process, especially parameters, such as capillary displacement pressure, relative permeability and displacement efficiency. The results indicate that CO_2 phase significantly affect their breakthrough. The breakthrough took place with the least volume of injected liquid CO_2 (LCO_2), and with the largest volume of gas CO_2 (gCO_2). The capillary displacement pressure can be measured based on the jumps in the pressure profiles, and it shows the largest jump in gCO_2 drainage. The relative permeability is the largest in LCO_2-water displacement and the smallest in gCO_2-water displacement. The displacement efficiency can be improved by increasing capillary number when it is smaller than a critical value around 2×10^{-8}.

Keywords: CO_2 phase; CO_2 breakthrough time; capillary displacement pressure; relative permeability; water recovery

1. Introduction

CO_2 storage in reliable reservoirs, aquifers and unminable coal seams has been seen as a promising technology to reduce CO_2 emissions into atmosphere (Safi et al., 2016; Shi and Durucan, 2005). As the pressure and temperature in these formations vary with the depth of the reservoirs, the stored CO_2 can be in different phases (Saraji et al., 2014). In formations with a temperature lower than 30.98 °C, CO_2 can be in gaseous state (gCO_2) e.g., Alabama Black Warrior Basin ~ 70 bar, 23 °C, or in liquid state (LCO_2), for instance West Sak reservoir ~ 110-125 bar, 24 °C. While in a formation with a temperature higher than 30.98 °C, CO_2 can be in supercritical state (sCO_2), for instance, Weyburn oil field ~ 140 bar, 59 °C (Espinoza and Santamarina, 2010; Li et al., 2005; Saraji et al., 2014).

The process of injection, migration and storage of CO_2 in reservoirs, aquifers or unminable coal seams are significantly affected by the interfacial tension (IFT) and contact angle (CA) in the fluid-CO_2-mineral systems, fluid property, physical and chemical properties of pore surfaces, and pore structure, etc. (Sarmadivaleh et al., 2015). Previous research has demonstrated that the interfacial tension and contact angle of CO_2 on minerals in subsurface vary significantly with CO_2 phase, temperature and pressure (Bikkina, 2011; Espinoza and Santamarina, 2010). Chi et al. found that water-CO_2 contact angle on coal surface changed from 84 °C (hydrophilic) to 145 °C (hydrophobic) when CO_2 varied from gas phase to liquid phase (Chi et al., 1988). Jung et al. (Jung and Wan, 2012) observed a sudden increase in water-CO_2 contact angle on silica surfaces when CO_2 phase changed from gas to supercritical state. Similar phenomenon was observed from the measurement of CO_2-water contact angle in single capillaries. Li et al. (Li and Fan, 2015) experimentally demonstrated that the CO_2-fluid contact angles vary considerably with CO_2 phase in oil-wet pores, but not in water-wet pores. Besides contact angles, intensive investigations focus on the effect of CO_2 phase on interfacial tension between CO_2 and water/Brine under various temperature and pressure. Espinoza et al. and Bachu et al. have demonstrated that interfacial tension between CO_2 and water decreases greatly with increase of CO_2 pressure at room temperature (298 K), and remains almost constant at the CO_2 vapour-liquid boundary (Bachu and Bennion, 2008; Espinoza and Santamarina, 2010). This trend has

been further confirmed by molecular dynamics computations (Iglauer et al., 2012). Therefore, CO_2 phase could have a notable influence on capillary entry pressure, displacement pressure, differential pressure, displacement efficiency, relative permeability and storage capacity, etc. (Krevor et al., 2012; Riazi et al., 2011).

Numerous research work has been designed to investigate CO_2 breakthrough (BT) time, capillary pressure, relative permeability and sub-core scale heterogeneity, etc. (Hildenbrand et al., 2002; Perrin and Benson, 2010; Wang and Alvarado, 2016). In CO_2 dynamic displacement, CO_2 breakthrough time, usually represented by the amount of CO_2 injected, is an important parameter and has significant effect on displacement efficiency, the calibration of real time production profile and the determination of relative permeability (Cao et al., 2014). For example, an early gas breakthrough at CO_2 enhanced oil recovery (EOR) could lead to poor sweep efficiency and the reduction of oil production (Gozalpour et al., 2005). In traditional measurements, breakthrough time is usually determined by the turning point on the differential pressure profiles as the production of the first-oil or the first-water in displacement experiment is invisible (Liang et al., 2016). However, it is sometimes hard to find the turning point under a low injection rate or in a high permeability core with little differential pressure change (Liang et al., 2016), and it is hard to determine the breakthrough time in a heterogeneous core with a complex differential pressure (Perrin and Benson, 2010). The method frequently used to determine the breakthrough time is CT scan through visualising changes in situ saturation distribution during core flooding experiments (Perrin et al., 2009). Shi et al. observed a CO_2 breakthrough by CT images after 0.42 pore volume (PV) of supercritical CO_2 was injected into a heterogeneous water-saturated Tako sandstone (Shi et al., 2011). Liang et al. designed a two phase detector probe connected to outflow endcap of core holder to identify the CO_2 breakthrough time for oil-water unsteady-state displacement experiments (Liang et al., 2016). Once the CO_2 breakthrough time is determined, the relative permeability of CO_2 and water/oil in the unsteady state displacement can be estimated through JBN method based on Buckley-Leverett theory (Buckley and Leverett, 1942; Johnson et al., 1959). JBN method is more efficient than steady method to get relative permeability curve with

continuous saturation distribution. Steady method can get only one point each time (Liu et al., 2010). Xu et al. used the JBN method to predict the relative permeability of sCO_2 and water in the process of injecting sCO_2 into porous media containing water. The predicted results showed a good agreement with the experimental data (Xu et al., 2011). Liu et al. modified JBN method by considering capillary pressure gradient to calculate the relative permeability of oil and water for particular low permeability reservoirs. Their results showed that the modified JBN method can predict the relative permeability more accurately than empirical formula for extra low permeability Reservoir (Liu et al., 2010). Chen et al. extended the JBN method to obtain relative permeabilities of CO_2 and brine at each pressure tap of the core (not just at the core outlet) by measuring the section-wise pressure drop, local saturation and local phase fluxes (Chen et al., 2016).

However, most research work has focused on single phase of CO_2, especially supercritical CO_2 in core flooding experiments. For example, Tokunaga et al. measured the drainage and imbibition capillary pressure for supercritical CO_2 and brine in quartz sand and found that wettability of silica surfaces was influenced by the exposure time to sCO_2 (Tokunaga et al., 2013). Parvazdavani et al. showed that the relative permeability of gCO_2 and oil calculated by JBN method was similar to the results predicted by sophisticated inverse modelling method when the sandstone was highly fractured (Parvazdavani et al., 2017). Though the effect of CO_2 phase on the differential pressure and water production in a core flooding experiment was studied by Ebraheam et al. (Al-Zaidi et al., 2018), the understanding of its impact on the drainage process, especially essential parameters, such as CO_2 breakthrough time, capillary displacement pressure, relative permeability and displacement efficiency, is still limited.

In this study, unsteady-state drainage experiments in a sandstone core sample was designed to investigate the effect of CO_2 phase on the drainage process, especially flow parameters, such as CO_2 breakthrough time, capillary displacement pressure and relative permeability. A simple and effective method was proposed to determine the CO_2 breakthrough through placing a membrane at the outlet of the core and the breakthrough point was found as the turning point

on differential pressure curve. The impact of CO_2 phase on the capillary displacement pressure was studied by comparing the pressure jumps on the pressure profiles. The effect of CO_2 phase on the relative permeability of water displacement were measured and compared with JBN method. The uncertainties of relative permeabilities were also assessed. The relevance between water recovery and capillary number was finally examined to investigate the effects of viscous and capillary forces on the displacement efficiency.

2. Materials and experimental setup

Sandstone core samples were provided by Anasuria Operating Company, UK. Double deionized water was used with an electrical resistivity greater than 18.18 MΩ·cm. Dry CO_2 was supplied by BOC with a guaranteed minimum purity level 99.995% in a cylinder fitted with a dip tube to permit withdrawal of liquid phase of CO_2.

2.1. Core sample

The core plug sample used for CO_2 flooding experiment has a diameter of 2.3 cm and a length of 3.7 cm and an average porosity of 0.23. The absolute permeability of the core sample was measured by DI water under different confining pressure and at a flowrate range from 0.05 to 0.4 mL/min, as shown in Fig. 1. The results are fitted linearly and the permeability can be derived from the slope by Darcy's law, which are 152, 138 and 129 mD (1 mD = 10^{-15} m^2) under confining pressures of 1000, 1500 and 2000 PSI respectively. The reduction of permeability under high confining pressure could be caused by the closure of the elliptic pores rather than the presence of fractures (Shi et al., 2011). All other experiments were conducted at the same confining pressure (2000 PSI) to keep a consistent permeability of the core (129 mD). The wettability of the core sample was measured with a Drop Shape analyser (DSA 100). 10 μL of ultrapure water with 18.2 MΩ·cm was placed on the surface of the air-saturated (dry) core at ~ 20 °C by a pipette and then a photographic digital image of the droplet on the surface was taken by DSA 100. After setting the baseline, the air-liquid-rock contact angle calculated was around 77 ° by the software, which showed that the core sample was hydrophilic. In Li's work,

the CO_2-fluid contact angles were independent of CO_2 phase in a water-wet pore (Li and Fan, 2015).

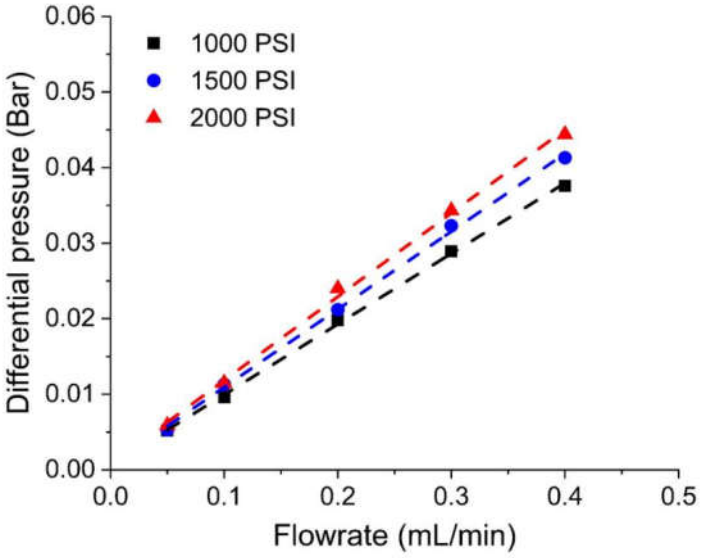

Fig. 1. The differential pressure versus flowrate under different confining pressures.

2.2. Experimental setup

An unsteady-state core flooding system was designed for CO_2-water dynamic displacement experiments, which is shown in Fig. 2. The system is consisted of two high-pressure (up to 695 bar) syringe pumps (ISCO syringe pump, 100DM) with a flowrate ranging from 0.00001 to 30 ml/min for CO_2 injection and water collection, an overburden-pressure water pump (Milton Roy, CM4000) to create the confining pressure, a vacuum pump to remove trapped gas, a core holder with a shrinkable Teflon sleeve to place the core plug and a hot water bath (Grant Instruments, GD100) to control the temperature with a precision of ± 0.02 °C. A LabVIEW software was built to automatically record the data of inlet and outlet pressure which was measured by two pressure transducers (UNIK, 100 bar gauge with a precision of ± 0.001 bar).

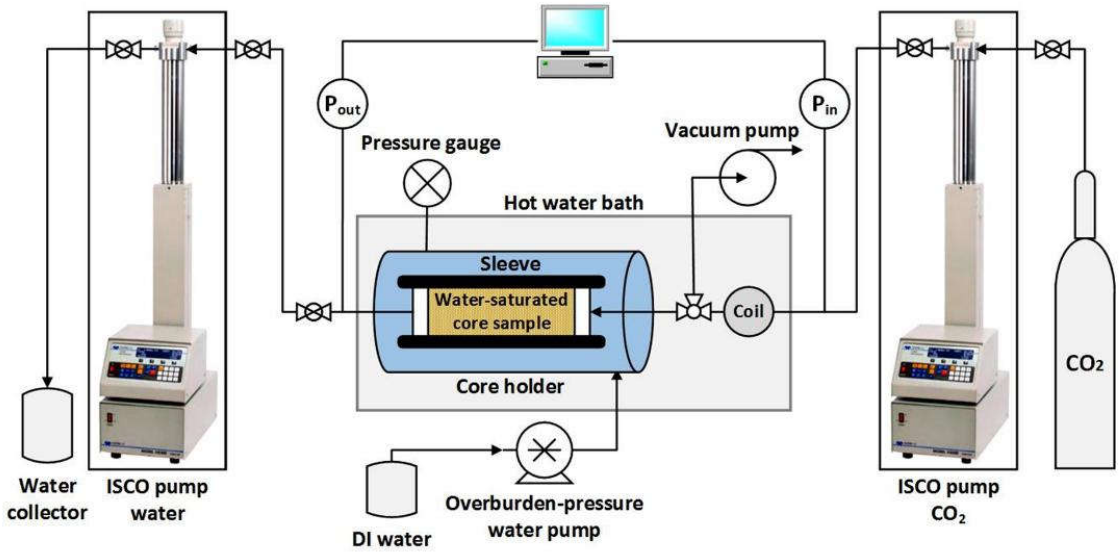

Fig. 2. Schematic diagram of CO_2 core flooding system.

Table 1. Operating conditions of the experiments.

Pressure (Bar)	Temperature (°C)	Phase state	Flowrate (mL/min)	IFT of CO_2 and water (mN/m)	Viscosity ratio (CO_2/water)	Capillary number N_{ca}(×10^{-8})
45	17	Gas	0.1-0.3	40.4	0.015	0.7-2.1
80	40	Supercritical	0.1-0.3	31.3	0.035	1.4-4.3
80	22	Liquid	0.1-0.3	29.8	0.075	4.3-12.8

2.3. CO_2-water displacement procedure

Experiments were conducted under various reservoir conditions where CO_2 can be in different phases. CO_2 injection flowrate was in a range from 0.1 to 0.3 mL/min, which correspond to a superficial flow velocity of 4 to 12 µm/s. For each experiment, the injection flowrate was constant. The experimental conditions are presented in table 1. The interfacial tension between water and CO_2 is obtained from literature (Bachu and Bennion, 2008) and the viscosities of water and CO_2 are available from NIST CHEMISTRY Webbook website (Chase Jr and Tables, 1998).

The core plug was pre-saturated with pure water and then wrapped in a shrinkable rubber sleeve and placed in a horizontal core holder. The core holder was immersed in the hot water bath and kept at a targeted temperature for several hours to achieve the thermal equilibrium. The confining pressure, 13.79 MPa (2000 psi), which was always larger than pore pressure, was firstly built by the overburden-pressure water pump to ensure the tight fitting between the rubber sleeve and the core sample, and thus to prevent fluid bypassing through the space between the rubber sleeve and the outside of the core (Shiraki and Dunn, 2000). Prior to the core flooding experiment, at least 30 pore volume of pure water was injected by syringe pump into the core at a high flowrate of 20 mL/min to remove the air in the system and to dissolve any CO_2 present in the core, and thus to ensure a complete saturation of the core with water (Kyte et al., 1956; Narayanan et al., 2018). Some more water was injected into the core to build the back pressure. After removing the trapped air by the vacuum pump, CO_2 was injected at the targeted pressure by the syringe pump (the CO_2 injecting pump in Fig. 2) into the inlet pipe. A coil placed at the inlet was to ensure that CO_2 was achieved thermal balance before it entered into the core sample. Keeping the system balanced at the targeted pressure for an hour, the core flooding experiment was then started by switching the CO_2 injection syringe pump from constant pressure to constant flowrate. During the experiment, the transient data of inlet pressure, outlet pressure and production of water and CO_2 was carefully monitored. The inlet and outlet pressures were measured by two pressure transducers and automatically recorded every 6 seconds, by the LabVIEW software, which were later used to calculate the differential pressure across the core sample. Another water syringe pump was used to collect the production of water and CO_2. The cumulative production volume of water and CO_2 was recorded every minute. Each experiment was terminated after injecting about 2 pore volume of CO_2. After each experiment, the weight of the core was measured using the Sartorius weighing scale with a resolution of 0.0001 g to calculate the residual water saturation.

2.4. Baseline of the differential pressure

In order to have a clear observation of the evolution of the differential pressure when CO_2 started to flow within core sample, around 0.7 mL water was kept in the inlet prior to CO_2

injection into the core. Before CO_2 entered the core, the differential pressure was dominated by single phase flow of water in the core and its value corresponded to viscous pressure loss of water flow. Once CO_2 arrived at the inlet of the core, the pressure in injected CO_2 built up to overcome the capillary pressure caused by the interfacial tension between water and CO_2. Pressure jumps were observed in all the CO_2-water displacement experiments regardless of what phase CO_2 was, which indicates the value of capillary displacement pressure as discussed in section 4.2.2.

3. Results

3.1 Differential pressure

During the CO_2-water displacement experiments, the inlet and outlet pressure of the core sample were recorded every 6 seconds. The temporal resolution has been proved to be sufficient to capture differences in fluid front configurations in dynamic flow experiments, such as Haines jumps (Berg et al., 2013). The differential pressures of drainage processes by different CO_2 phases are shown in Fig. 3. At injection flowrate ranging from 0.1 to 0.3 mL/min, the drainage process is a typical of slow capillary-dominated drainage with intermittent fluctuations (Primkulov et al., 2019). At the first stage of the experiments, the differential pressure is determined by water flow in the core sample as water prior to the inlet was pushed into the core sample by CO_2. This can be verified by the small pressure variation at the beginning of the profiles in Fig. 3(a)-(c). When CO_2 arrives at the inlet of the core sample, the pressures suddenly built up to overcome the capillary force caused by the CO_2-water interfacial tension. After CO_2 enters into the core sample, the pressure is dominated by evolution of CO_2-water interface, that is, cooperative pore filling events (like burst, touch or overlap) defined by Cieplak & Robbins (Cieplak and Robbins, 1988), resulting in the fluctuations on the pressure profiles.

It is worth to note that injection flowrate of CO_2 set by the injection pump is sometimes different from the CO_2 flowrate in the core sample as the temperature in the pump differs from that in the water bath. This leads to a variation in CO_2 density and CO_2 phase. For example, to obtain a CO_2 flowrate of 0.1 mL/min in the core at 40 °C and 80 Bar, the CO_2 flowrate in the

pump at room temperature and the same pressure needs to be set as $Q_p = \frac{\rho_{CO2}^{40°C\ 80Bar}}{\rho_{CO2}^{RT\ 80Bar}} \times 0.1$ mL/min.

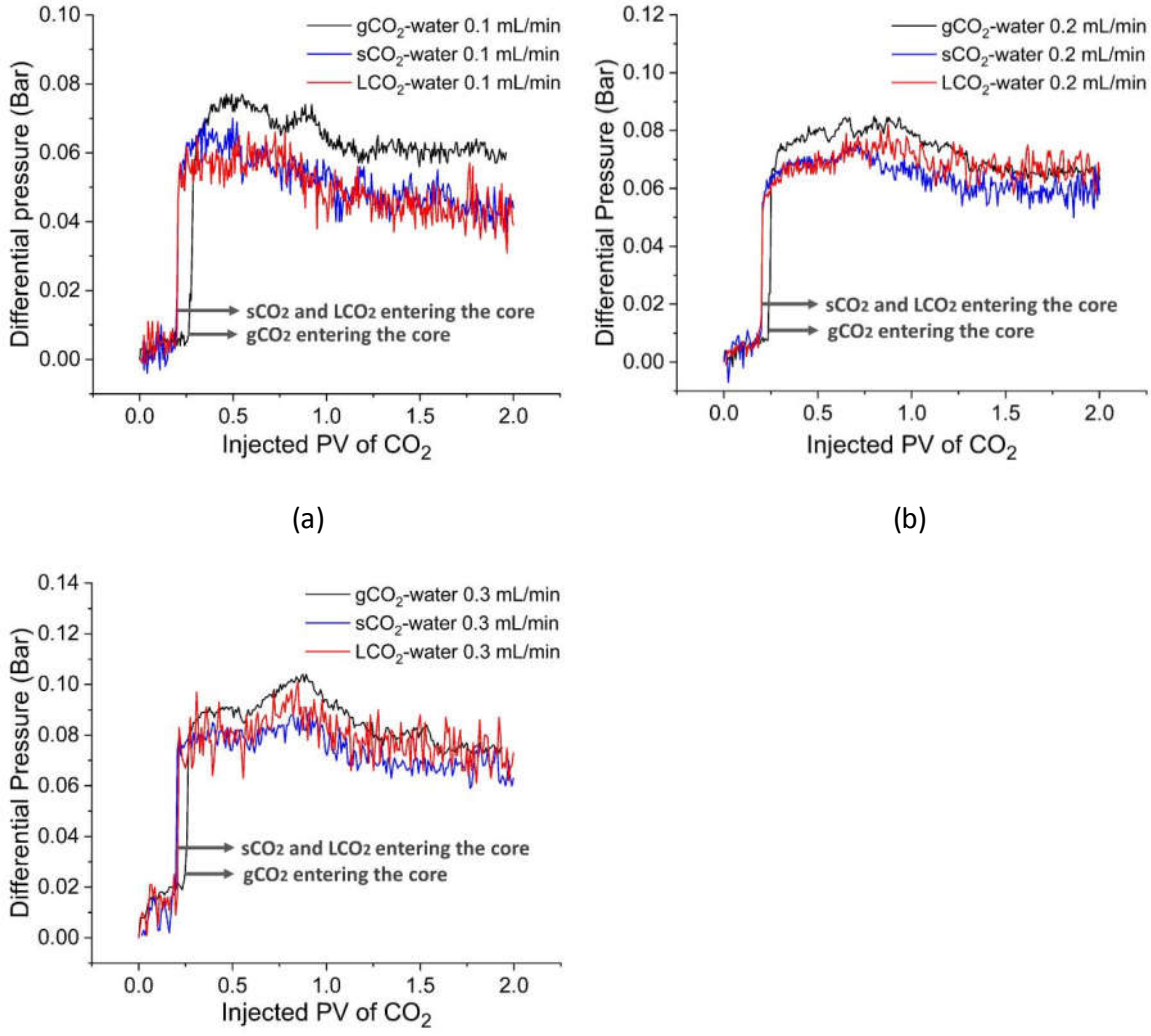

Fig. 3. Differential pressure across the core sample for the displacement of water by gCO_2, $scCO_2$ and LCO_2 at an injection flowrate of (a) 0.1 mL/min, (b) 0.2 mL/min and (3) 0.3 mL/min.

3.2 CO_2 and water production

CO_2 and water production were collected by the pump at the outlet of the core sample every minute. The effect of CO_2 phases on their production rate and cumulative production is presented in Fig. 4(a)-(c). The results indicate that the production rate and cumulative production vary significantly with CO_2 phases. For LCO_2-water displacement, the collective production rate is very close to the CO_2 injection flowrates and the production is always higher than that in gCO_2, sCO_2 injection processes. For gCO_2-water displacement, the production rate varies greatly during the injection process. Before CO_2 entering the core sample, the production rate increases quickly to the given injection flowrate. When CO_2 starts to enter the core, the production rate decreases rapidly as part of injected gas CO_2 has be compressed to build up the pressure. After the injection of around 1 PV CO_2, the production starts to be stabilized and close to the given injection flowrate. The cumulative production during gCO_2 injection is the smallest. The production rate and cumulative production of sCO_2 displacement varies between LCO_2 and gCO_2 displacement as its density, viscosity and compressibility, are between LCO_2 and gCO_2.

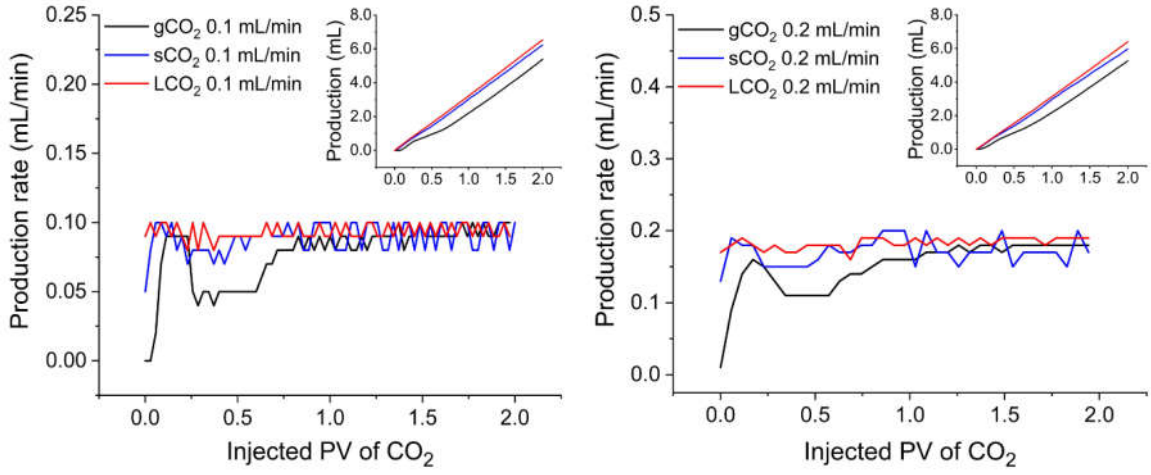

(a) (b)

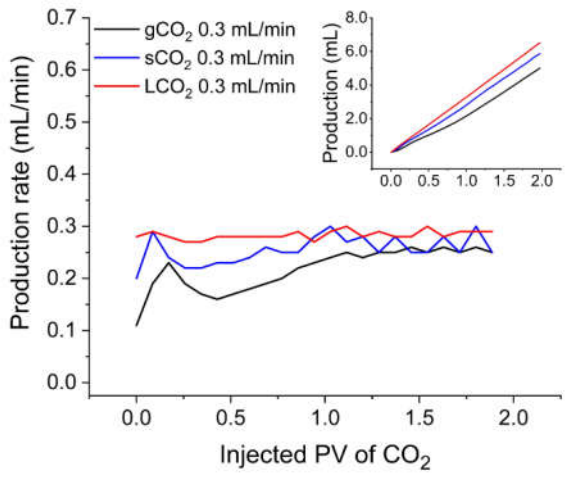

(c)

Fig. 4. Effect of CO_2 phase on water production rate and corresponding cumulative production (inset) during drainage process at an injection flowrate of (a) 0.1 mL/min, (b) 0.2 mL/min and (c) 0.3 mL/min.

4. Discussions

4.1. Determination of breakthrough time

An accurate identification of CO_2 breakthrough time is a first-line step for further determining parameters such as water/CO_2 fractional flow, relative permeability, and displacement efficiency. Though there is a straight and visualized way to observe CO_2 breakthrough by CT images, the core flooding rig equipped with CT is more complicated and expensive. An economic and convenient method present in this paper to determine the CO_2 breakthrough time is through placing a membrane (Nuclepore Track-Etch Membrane-Whatman) with a low permeability of ~ 0.01 mD at the outlet of the core sample. The breakthrough time can be easily seen from the differential profile of the core sample with a membrane.

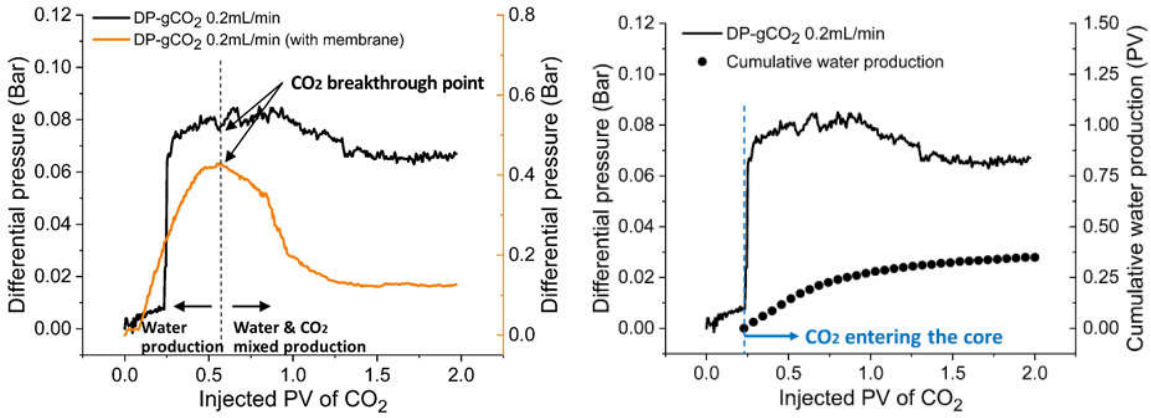

(a) (b)

Fig. 5. Take gas CO_2-water displacement at injection flowrate of 0.2 mL/min as an example to determine (a) CO_2 breakthrough time and (b) cumulative water production.

Taking gas CO_2-water displacement with 0.2 mL/min injection flowrate as an example (Fig. 5(a)), the black line is the original differential pressure across the core sample without a membrane and the yellow line is the differential pressure with a membrane. The application of the membrane gives very different differential pressure profiles for the flooding process. After the application of a membrane, the magnitude of the differential pressure is much larger than that in the original core sample, and there is a maximum value in the pressure profile. The time corresponding to the maximum value is the breakthrough time as shown in Fig. 5(a). This is due to the difference in the viscosity of water and CO_2.

The total differential pressure (ΔP_T) along the core sample and membrane is the sum of capillary pressure (P_c) and viscous pressure drop (ΔP_v), i.e.,

$$\Delta P_T = P_c + \Delta P_v \quad (1)$$

As the change of the capillary pressure is not obvious during the displacement in the core sample, the significant change in the differential profile for the core sample with a membrane (the yellow line in Fig. 5(a)) is contributed by the viscosity difference between water and CO_2. As the water viscosity is much larger than CO_2 viscosity, the viscous pressure drop of water through the membrane is much larger than CO_2. Once CO_2 reaches a breakthrough, CO_2

immediately enters into the membrane, and the pressure drop caused by viscosity drops significantly.

Applying Leverett extension of Darcy's law to multiphase flow in porous media, the pressure for each phase (*i=n, w)* is (Ramakrishnan and Chugunov, 2013),

$$\frac{\partial P_i}{\partial x} = -\frac{\mu_i}{KK_{ri}}\frac{Q_i}{A} \tag{2}$$

where *P*, μ, *Q* and *Kr* are the pressure, viscosity, volume flow rate and relative permeability for phase *i*. *K*, *A* and *x* are the intrinsic permeability, cross-sectional area and length of the porous media. The viscous pressure loss of each phase flowing across the membrane is approximately 50 times larger than that in core sample based on Eq. (2). The variation of the differential pressure is therefore largely dominated by the water and CO_2 flow through the membrane. The viscosity ratio between water and CO_2 varies significantly with CO_2 phase. The viscosity of water is 60, 30, 15 times larger than that of gCO_2, sCO_2 and LCO_2 respectively. The viscous pressure drop caused by water is much larger than CO_2. Once CO_2 enters into the membrane, the differential pressure across the membrane decreases as shown in Fig. 5(a). CO_2 breakthrough time thus can be clearly determined by the turning point on the differential pressure profile with a membrane. Among many factors, CO_2 breakthrough time depends critically on the relative permeability of each phase which relates to the distribution of permeability within a reservoir, injection flowrate and viscosity ratio of invading phase to displaced phase, etc. (Jessen et al., 2005). The variation of injection flowrate in this experiment hardly affected CO_2 breakthrough time and CO_2 breakthrough happened after 0.3, 0.23 and 0.19 pore volume of CO_2 was injected for gCO_2, sCO_2 and LCO_2-water displacement experiment, respectively.

Before CO_2 breakthrough, only water production was collected from the outlet, and after that, both CO_2 and water were collected until the equilibrium (steady-state) period when only CO_2 was collected as the water saturation in the core sample become irreducible. The water production before CO_2 breakthrough can be calculated from the increase volume of the receiving pump. After CO_2 breakthrough, the water production rate $v(t)$ can be correlated by the power-law equation (Toth et al., 2001; Toth et al., 2002),

$$v(t) = at^b \quad t \geq t_{BT} \tag{3}$$

where t is dimensionless time, a and b are constant parameters that can be determined by calculating the water production rate at the CO_2 breakthrough point and the integral of water production rate from CO_2 breakthrough to the end. The cumulative water production then can be calculated as shown in Fig. 5(b), which indicated most water production happened at the initial stage of CO_2 injection and it almost stabilized after injecting 1.5 PV of CO_2.

4.2. Effect of CO_2 phase on differential pressure

4.2.1. Pressure fluctuation

The differential pressure profiles are split into the general trend (red line) and fluctuation components (blue line) by wavelet decomposition, as shown in Fig.6 (a). The fluctuation has been explained by Bauyrzhan et al. (Primkulov et al., 2019). It is due to the reconfigurations of the CO_2-water interface when invading phase (CO_2) enters into the pores. However, their explanations are based on the numerical simulation, and it might be different from experiment. For example, before CO_2 enters into the core sample, some pressure fluctuation was also observed from the profiles. This may be caused by the running of the pump and intrinsic error of pressure transducer. The standard deviation of pressure fluctuation of CO_2-water flow has been presented in Fig. 6(b) and it shows that fluctuation is almost independent of injection flowrate but related to the CO_2 phase. LCO_2-water displacement has the largest pressure fluctuation while gCO_2-water displacement gives the smallest one. To invade the pores and push out of the defending fluid, the pressure needs to overcome the capillary pressure at the pore throat, which is controlled by Young-Laplace equation. The general form of the equation is,

$$P_c = \sigma_{CO_2,w} \times (\frac{1}{a} + \frac{1}{h}) \tag{4}$$

where $\sigma_{CO_2,w}$ is the IFT between CO_2 and water, a is the width of the pore throat and h is the height of the pore. During the displacement, the variation of P_c was dominated by the invaded pore size. Take the variation of P_c with a and h,

$$\delta P_c = \frac{\sigma_{CO_2,w}}{a^2}\delta a + \frac{\sigma_{CO_2,w}}{h^2}\delta h \tag{5}$$

Eq. (5) indicates that the pressure fluctuation is related to the interfacial tension between two fluids and the variation of a and h. A higher mobility ratio (μ_{CO2}/μ_{water}) usually favours

displacement, which means CO_2 can invade in more pores with smaller size (Lenormand et al., 1988). The mobility ratio of LCO_2-water displacement is much larger than gCO_2, sCO_2-water displacement, which therefore shows a larger fluctuation in differential pressure profiles.

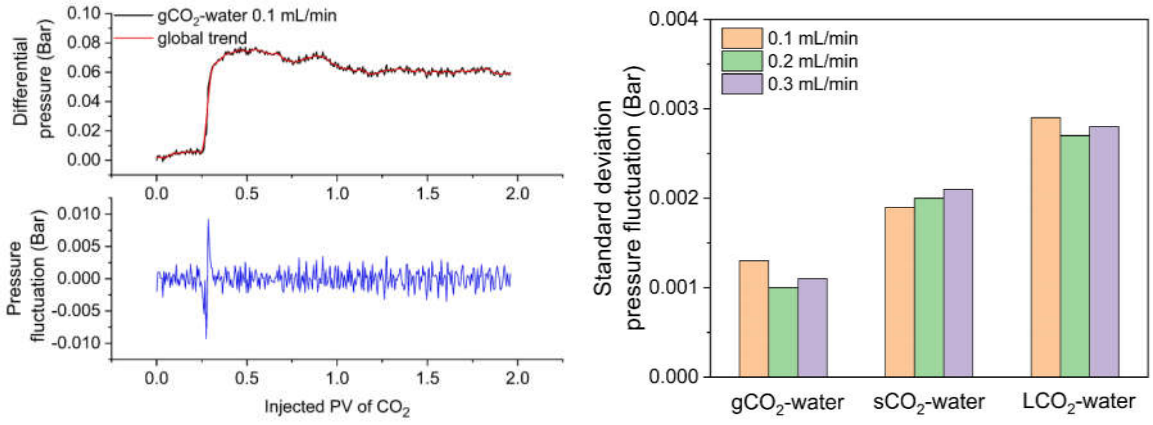

(a) (b)

Fig. 6. Wavelet decomposition analysis of the differential pressure: (a) splitting the pressure profile into global trend (red line) and fluctuation (blue line) and (b) standard deviation of pressure fluctuation for gCO_2, sCO_2 and LCO_2-water displacement at different injection flowrate.

4.2.2. Capillary displacement pressure

As mentioned in section 2.4, pressure jumps were observed in all CO_2-water displacement experiments. The values of pressure jumps are shown in Fig. 7, which are clearly independent on injection flowrate, but dependent on the CO_2 phase. In Egermann's experiment (Egermann et al., 2006), the value of the pressure jump observed at the moment when CO_2 initially entered into the core were close to displacement pressure (P_{cd}) derived from the mercury-injection curve. The capillary displacement pressure in a tube is caused by the curved interface between the non-wetting phase (CO_2) and wetting phase (water). It can be described by the modified Young-Laplace equation (Chalbaud et al., 2007),

$$P_{cd} = P_{CO_2} - P_{water} = \frac{2\sigma_{CO_2,w}\cos\theta}{R_{throat}^{\max}} \quad (6)$$

where P_{cd} is the capillary displacement pressure value, $\sigma_{CO_2,w}$ is the IFT between CO_2 and water, θ is the contact angle and $R_{throat}^{\max}$ corresponds to the largest connected pore throats.

The IFT between gCO_2 and water is usually larger than that between sCO_2 or LCO_2 and water as shown in Fig. 8, which leads to higher capillary displacement pressure for gCO_2 displacing water according to Eq. (6) and thus requires larger external pressure difference to overcome it. Assuming the core sample as a bundle of capillary channels with the same radius, the relationship between permeability and channel diameter was $K = \phi d^2/32\tau$ (Kozeny, 1927), where ϕ is the porosity of the porous media, d is the channel diameter and τ is tortuosity defined as the ratio of actual length of flow path in the porous medium to the length of flow path in the absence of porous medium. Assuming τ equals to unit, the estimated displacement pressure can be expressed as,

$$P_{cd}^{est} = \frac{2\sigma_{CO_2,w}\cos\theta}{\sqrt{2K/\phi}} \quad (7)$$

The estimated values of capillary displacement pressure from Eq. (7) is presented in Fig. 7. They are 28%, 25% and 27% larger than the experiment results in gCO_2-water, sCO_2-water and LCO_2-water displacement, respectively. The overestimation of the displacement pressure is because the pore size in Kozeny model is assumed as uniform, which is smaller than the size of largest pore throats of the core sample.

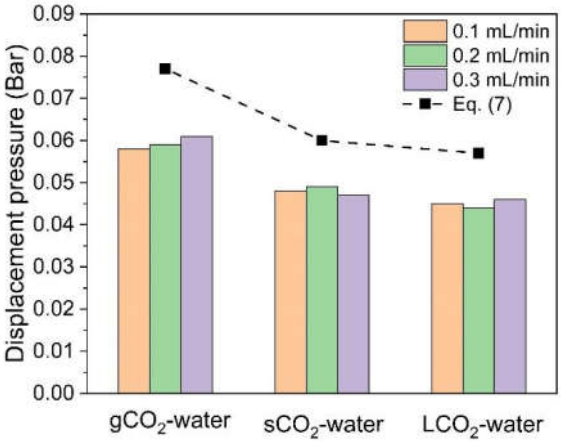

Fig. 7. Values of pressure jumps at the beginning of drainage and estimated capillary displacement pressure by Kozeny model (Kozeny, 1927)

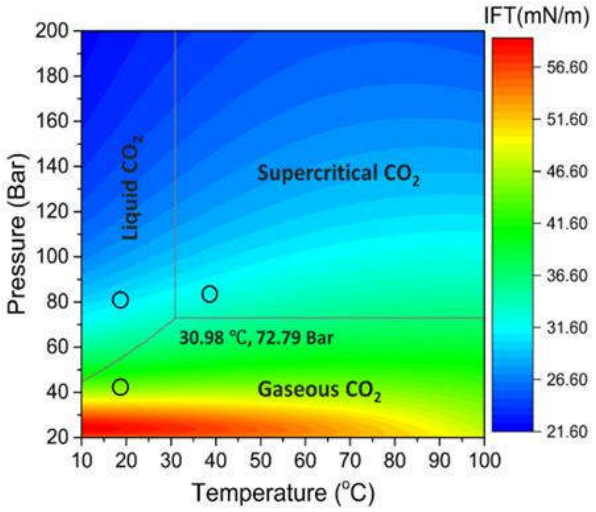

Fig.8. A contour map of CO_2-water IFT as a function of pressure and temperature calculated from equations in literature (Li et al., 2012). Our experimental conditions are shown by the circles.

4.3. Effect of CO_2 phase on the relative permeability

Relative permeability is a vital parameter in subsurface hydrology. It reflects the capability of a specific formation to produce a combination of oil, water or gas more accurately than the absolute permeability under multiphase flow conditions (Chen et al., 2016). The JBN method is a popular method and can be used to quickly determine the relative permeability of the invading phase (CO_2) and the defending phase (water) at the outlet of the core sample across a range of saturations. To apply this method to the unsteady-state drainage experiments, we assume (Johnson et al., 1959): (1) stabilized displacement can be satisfied with high enough flow velocity and (2) incompressible fluids can be obtained by maintaining gas phase at a high enough pressure level (Johnson et al., 1959). During displacement, the differential pressure across the core sample and the phase fractional flow need to be measured. By applying generalized Darcy's law and fractional flow equation to Buckley-Leverett theory (continuity equation) with those assumptions, relative permeability of CO_2 and water and CO_2 saturation at the outlet of the core can be calculated as Eqs. (8)-(11) (Buckley and Leverett, 1942; Johnson et al., 1959),

$$f_{w,2} = \frac{dS_{CO_2,av}}{dt_d} \tag{8}$$

$$K_{rw,2} = \frac{f_{w,2} L Q_i \mu_w}{KA} \frac{d(1/t_d)}{d(\Delta P/t_d)} \quad (9)$$

$$K_{rCO_2,2} = k_{rw,2} \frac{\mu_{CO_2}}{\mu_w} \frac{(1-f_{w,2})}{f_{w,2}} \quad (10)$$

$$S_{CO_2,2} = S_{CO_2,avg} - f_{w,2} t_d \quad (11)$$

where subscript 2 denotes the outlet of the core; $f_{w,2}$ is fractional flow of water at the core outlet; $S_{CO_2,av}$ is the average CO_2 saturation of the core; t_d is dimensionless time indicated by injected pore volume; $K_{rw,2}$ and $K_{rCO_2,2}$ represent relative permeability of water and CO_2 at the core outlet respectively; Q_i is volumetric injection flowrate; μ_w is viscosity of water; ΔP is the measured pressure difference across the core; K, A and L are absolute permeability, cross section area and length of the core, respectively; $S_{CO_2,2}$ and $S_{CO_2,av}$ are core outlet and core-average CO_2 saturation, respectively.

Rapoport (Rapoport and Leas, 1953) suggested a scaling coefficient of $\mu_w L Q_i / \mathrm{A}$ ($\frac{cm^2}{min} \cdot cP$) to evaluate the capillary end effect. If the coefficient is larger than 0.1, it is applicable to assume the flow is stabilized. In this experiment, the coefficient ranges from 0.1 to 0.3, stabilised flow conditions can be achieved during the drainage. The incompressible condition assumes the inlet injection flowrate equals to the outlet production flowrate ($Q_i = Q_o$). However, the measured flowrate from outlet is smaller than the injection flowrate, especially in gCO_2-water displacement. Therefore, the uncertainty of relative permeability determined by this method can be assessed as,

$$\delta K_{rw,2} = \frac{f_{w,2} L \mu_w}{KA} \frac{d(1/t_d)}{d(\Delta P/t_d)} \frac{(Q_i - Q_o)}{Q_i} \quad (12)$$

$$\delta K_{rCO_2,2} = \frac{\mu_{CO_2}}{\mu_w} \frac{(1-f_{w,2})}{f_{w,2}} \delta K_{rw,2} \quad (13)$$

Relative permeability curves of CO_2 and water are shown in Fig. 9(a)-(c) at an injection flowrate from 0.1 mL/min to 0.3 mL/min. The error bars indicate the uncertainty of the relative permeability caused by the assumption of incompressible fluids. Larger uncertainty appears at smaller CO_2 saturation. gCO_2-water displacement always gives the largest uncertainty because gaseous CO_2 was compressed to build up the capillary pressure at the beginning of displacements. During the drainage process, LCO_2-water displacement always gives the largest

relative permeability for both water and CO_2 while the relative permeability of gCO_2-water displacement is smallest under the same injection flowrate condition. Eq. (9) indicates that the water relative permeability is mainly related to water fractional flow, water viscosity and differential pressure. As pressure difference across a high permeability core in the drainage process changes slightly, its influence on the relative permeability is insignificant (Liang et al., 2016). The differences between the relative permeability of water in different CO_2 phase core flooding is mainly caused by the water fraction flow. Fig. 10(a)-(c) present the fractional flow of water versus CO_2 saturation at various injection flowrate in different CO_2 phase displacements. It can be noted that the value of water fractional flow is greatest in LCO_2-water displacement and lowest in gCO_2-water displacement at the same CO_2 saturation under the same injection flowrate condition. According to Eq. (10), the low CO_2 relative permeability is mainly caused by the large difference between the viscosity of CO_2 and water. Besides, it is found that the injection flowrate hardly affects the relative permeability for both water and CO_2 in different CO_2 phase drainage processes, which is also proved in previous study (Chen and Wood, 2001). Therefore, the relative permeability obtained from the laboratory experiments can be also applied to the reservoir condition where the injection flowrate is smaller.

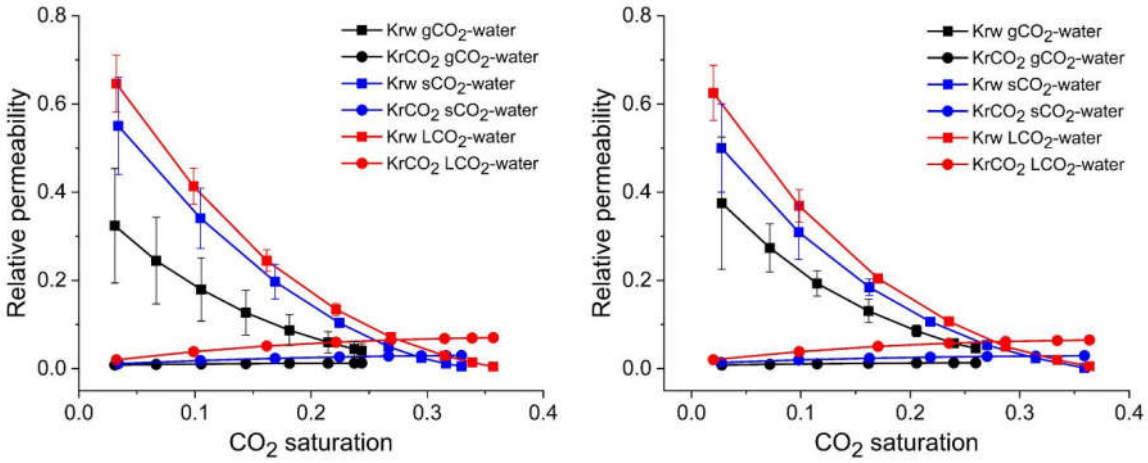

(a) (b)

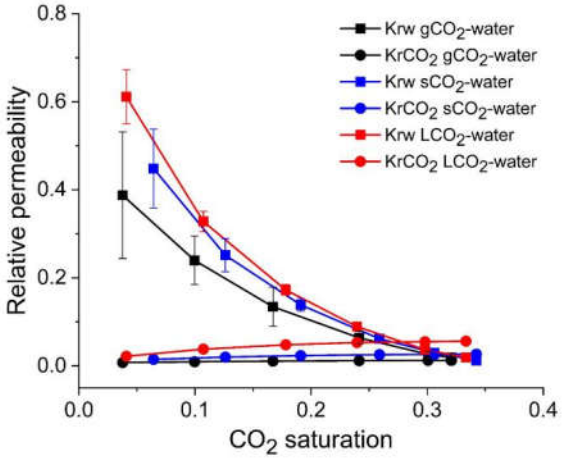

(c)

Fig. 9. Effect of CO_2 phase on the relative permeability in displacement of water at injection flowrate of (a) 0.1 mL/min, (b) 0.2 mL/min and (c) 0.3 mL/min.

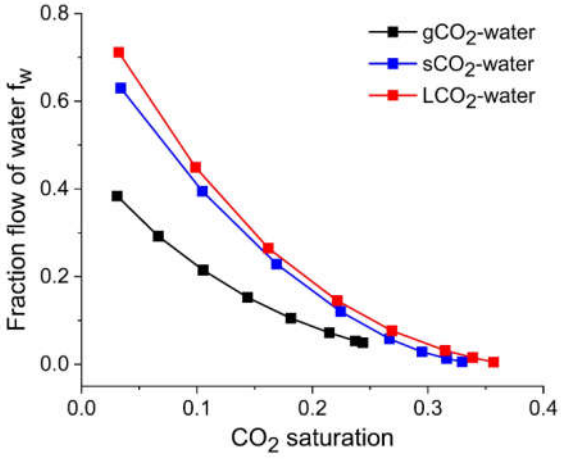

(a)

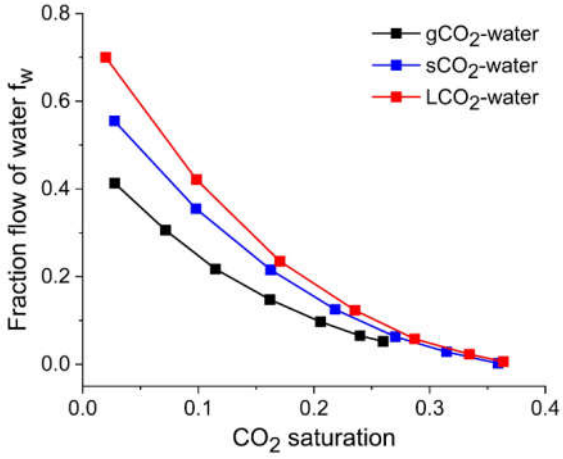

(b)

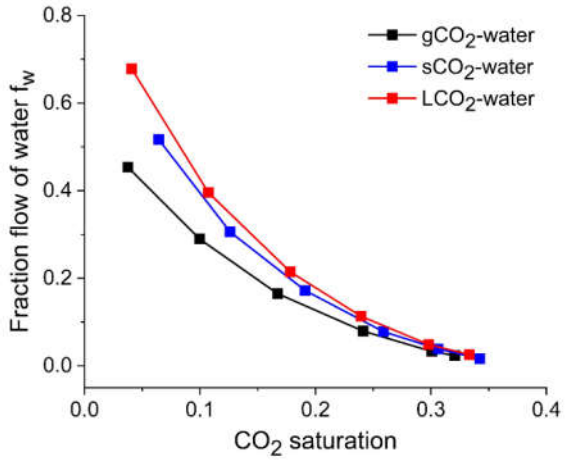

(c)

Fig. 10. Effect of CO_2 phase on water fractional flow in displacement of water at injection flowrate of (a) 0.1 mL/min, (b) 0.2 mL/min and (c) 0.3 mL/min.

4.4. Relationship between water recovery and capillary number

The method to calculate the water production was discussed in section 3.1. Fig. 11(a)-(c) show the cumulative water production denoted by the pore volume as a function of CO_2 injected pore volume at an injection flowrate varying from 0.1 mL/min to 0.3 mL/min. The results indicate that the cumulative water production reaches its maximum after injecting ~ 2 pore volumes of CO_2 and the displacement of water by LCO_2 gives the highest water production, while gCO_2-water displacement gives the lowest the water production CO_2. Commonly, the cumulative water production increases fast at the beginning (around CO_2 breakthrough point), and the growth rate slows down with the rise of injected CO_2 volume as water in larger pores is easily driven out first (Duan et al., 2016). Fig. 11(d) presents the terminal water production represented in PV as a function of injection flowrate. It is worthwhile to note that the ultimate water production increases with the increase of CO_2 injection flowrate, while the increasing trend tends to slow down. This is mainly because initial rise of injection flowrate could increase viscous force to push out the water which is occupying in large pores dominated by small capillary force. Further increasing flowrate would be more difficult to drive out the water remaining in small pores due to the large capillary force (Nobakht et al., 2007).

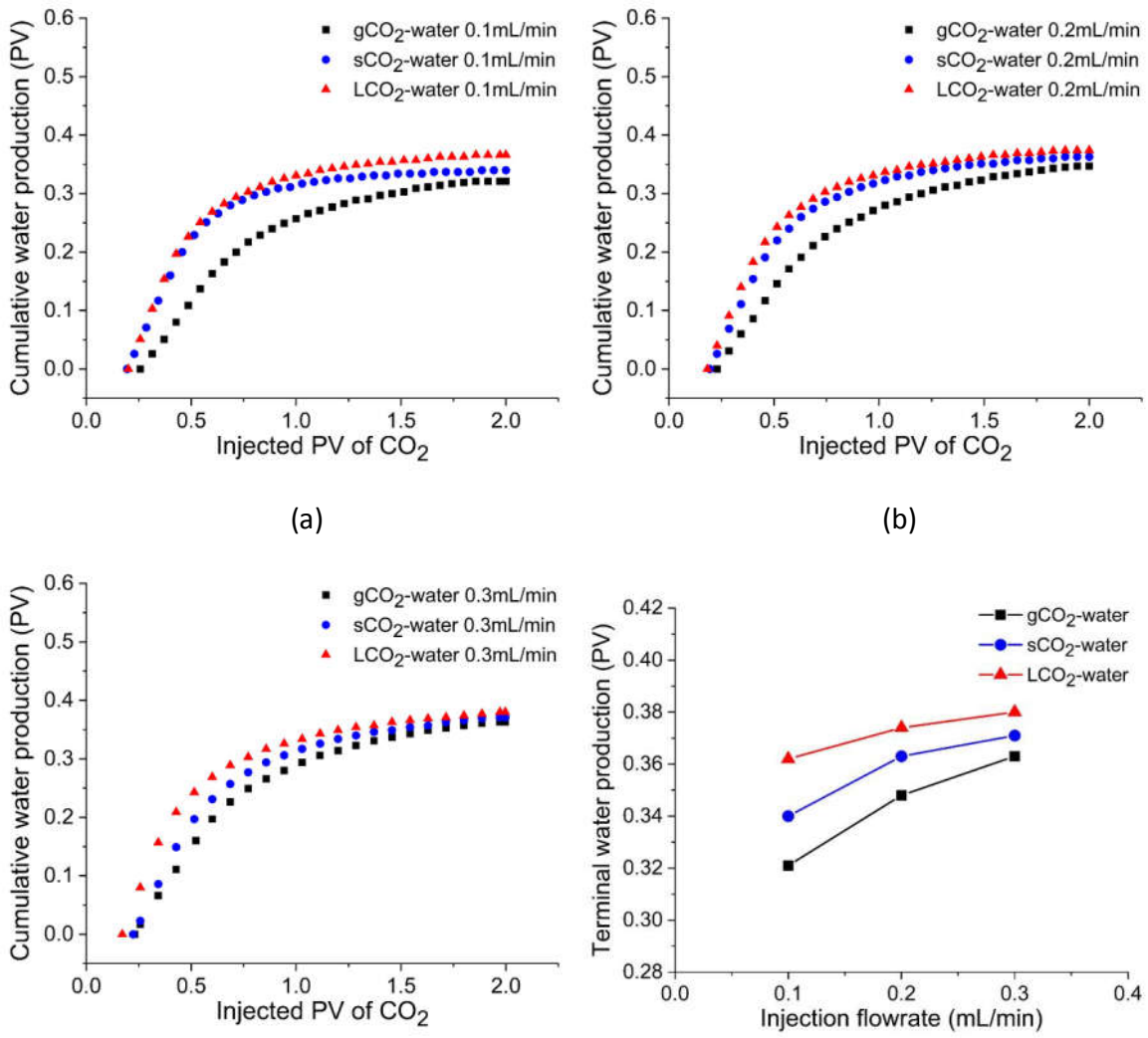

Fig. 11. Impact of CO_2 phase on water production as a function of injected pore volume of CO_2 at injection flowrate of (a) 0.1 mL/min, (b) 0.2 mL/min, (c) 0.3mL/min and (d) terminal water recovery as a function of injection flowrate.

In general, a two-phase flow in horizontal core sample is controlled by the capillary force and viscosity force. The quantitative relative effect between them can be evaluated as,

$$\frac{P_{vis}}{P_{cap}} \sim \frac{\mu v r/K}{\sigma/r} = \frac{r^2}{K} N_{ca} \tag{11}$$

where *r* is the grain size and *K* is the permeability of the core sample. The typical grain size is in order of 100 μm and the permeability in this experiment is about 100 mD. Thus, the value of

r^2/K is around 10^5 and for capillary number N_{ca} around 10^{-5}, viscous and capillary force are about the same. In this study, the capillary number $N_{ca} = \frac{v_{CO2}\mu_{CO2}}{\sigma_{CO2,w}}$, given in terms of invading phase (CO_2), is ranging roughly between 10^{-9} between 10^{-7}, which suggests that capillary forces are more important. Fig. 12 shows the effect of capillary number on water recovery. The water recovery is defined as the ratio of cumulative water production volume to pore volume of the core. The results indicate that water recovery increases generally with the capillary number though the growth rate seems different. When N_{ca} is smaller than ~ 2×10^{-8}, water recovery increases notably with the increase of capillary number because some water still remains in large pores after CO_2 flooding with small viscosity number. The increased viscous force pushes out more water. When N_{ca} is larger than ~ 2×10^{-8}, the increase rate in water recovery slows down, as most unrecovered water remains in smaller pores after flooding with larger viscous force. Further increasing viscous force is hardly to overcome the strong capillary force to drive the remaining water out (Nobakht et al., 2007). Therefore, increasing capillary number is a more effective way to increase the displacement efficiency when the capillary number is smaller than ~ 2×10^{-8}.

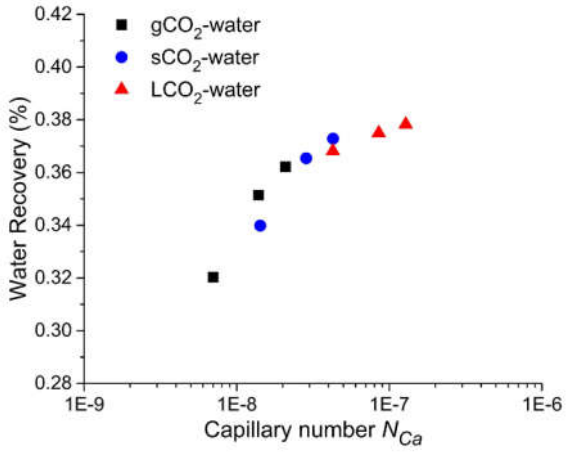

Fig. 12. Water recovery as a function of capillary number

5. Conclusions

The impact of CO_2 phase on the drainage process, especially the key parameters, such as CO_2 breakthrough time, capillary displacement pressure, relative permeability and displacement efficiency, has been thoroughly investigated in this study. The results indicate that:

1) CO_2 breakthrough point can be obtained from the turning point on the differential pressure curve by placing a low permeability membrane at the outlet of the core sample. The breakthrough is affected notably by CO_2 phase, but is independent of injection flowrate. The breakthrough happened earliest in LCO_2-water displacement, while it happened latest in gCO_2-water displacement.
2) The differential pressure fluctuates remarkably in LCO_2 drainage, but it is much smoother in gCO_2 drainage. The capillary displacement pressures for gCO_2, sCO_2 and LCO_2-water displacement are 0.059, 0.048 and 0.046 Bar, which are indicated by the pressure jumps and their values close to the results estimated by Kozeny model.
3) The relative permeability varies greatly with CO_2 phase, but is affected hardly by CO_2 injection flowrate. At the same injection flowrate, LCO_2-water displacement gives the largest relative permeability while gCO_2-water displacement has the smallest relative permeability. The uncertainty of relative permeability caused by incompressible assumption is largest for gCO_2-water displacement, especially at the beginning of the drainage.
4) CO_2 phase significantly affects the cumulative water production. LCO_2-water displacement gives the highest cumulative water production, while gCO_2-water displacement gives the lowest one at the same injection flowrate. Water recovery generally increases with the increase of N_{ca}. It increases remarkably when N_{ca} is smaller than ~ 2×10^{-8} and after which the growth trend slows down.

Acknowledgements

Authors gratefully acknowledge the financial supports from Chinese Scholarship Council (CSC) and UK India Education & Research Initiative (UKIERI).

Reference

Al-Zaidi, E., Nash, J., Fan, X., 2018. Effect of CO2 phase on its water displacements in a sandstone core sample. International Journal of Greenhouse Gas Control 71, 227-238.
Bachu, S., Bennion, D.B., 2008. Interfacial tension between CO2, freshwater, and brine in the range of pressure from (2 to 27) MPa, temperature from (20 to 125) C, and water salinity from (0 to 334 000) mg· L− 1. Journal of Chemical & Engineering Data 54, 765-775.
Berg, S., Ott, H., Klapp, S.A., Schwing, A., Neiteler, R., Brussee, N., Makurat, A., Leu, L., Enzmann, F., Schwarz, J.-O., 2013. Real-time 3D imaging of Haines jumps in porous media flow. Proceedings of the National Academy of Sciences 110, 3755-3759.
Bikkina, P.K., 2011. Contact angle measurements of CO2–water–quartz/calcite systems in the perspective of carbon sequestration. International Journal of Greenhouse Gas Control 5, 1259-1271.
Buckley, S.E., Leverett, M., 1942. Mechanism of fluid displacement in sands. Transactions of the AIME 146, 107-116.
Cao, J., James, L.A., Johansen, T.E., 2014. Determination of two phase relative permeability from core floods with constant pressure boundaries, Society of Core Analysis Symposium, Avignon, France.
Chalbaud, C.A., Lombard, J.-M.N., Martin, F., Robin, M., Bertin, H.J., Egermann, P., 2007. Two Phase Flow Properties of Brine-CO2 Systems in a Carbonate Core: Influence of Wettability on Pc and kr, SPE/EAGE Reservoir Characterization and Simulation Conference. Society of Petroleum Engineers.
Chase Jr, M.W., Tables, N.-J.T., 1998. Data reported in NIST standard reference database 69, June 2005 release: NIST Chemistry WebBook. J. Phys. Chem. Ref. Data, Monograph 9, 1-1951.
Chen, A., Wood, A., 2001. Rate effects on water-oil relative permeability, Proceedings of the International Symposium of the Society of Core Analysts, Edinburgh, Scotland, pp. 17-19.
Chen, X., Kianinejad, A., DiCarlo, D.A., 2016. An extended JBN method of determining unsteady-state two-phase relative permeability. Water Resources Research 52, 8374-8383.
Chi, S., Morsi, B., Klinzing, G., Chiang, S., 1988. Study of interfacial properties in the liquid carbon dioxide-water-coal system. Energy & Fuels 2, 141-145.
Cieplak, M., Robbins, M.O., 1988. Dynamical transition in quasistatic fluid invasion in porous media. Physical review letters 60, 2042.
Duan, X., Hou, J., Zhao, F., Ma, Y., Zhang, Z., 2016. Determination and controlling of gas channel in CO 2 immiscible flooding. Journal of the Energy Institute 89, 12-20.
Egermann, P., Chalbaud, C.A., Duquerroix, J., Le Gallo, Y., 2006. An integrated approach to parameterize reservoir models for CO2 injection in aquifers, SPE Annual Technical Conference and Exhibition. Society of Petroleum Engineers.
Espinoza, D.N., Santamarina, J.C., 2010. Water-CO2-mineral systems: Interfacial tension, contact angle, and diffusion-Implications to CO2 geological storage. Water Resources Research 46.
Gozalpour, F., Ren, S., Tohidi, B., 2005. CO2 EOR and storage in oil reservoir. Oil & gas science and technology 60, 537-546.

Hildenbrand, A., Schlömer, S., Krooss, B., 2002. Gas breakthrough experiments on fine‐grained sedimentary rocks. Geofluids 2, 3-23.
Iglauer, S., Mathew, M., Bresme, F., 2012. Molecular dynamics computations of brine–CO2 interfacial tensions and brine–CO2–quartz contact angles and their effects on structural and residual trapping mechanisms in carbon geo-sequestration. Journal of Colloid and Interface Science 386, 405-414.
Jessen, K., Kovscek, A.R., Orr Jr, F.M., 2005. Increasing CO2 storage in oil recovery. Energy Conversion and management 46, 293-311.
Johnson, E.F., Bossler, D.P., Naumann, V.O., 1959. Calculation of Relative Permeability from Displacement Experiments. Transactions of the American Institute of Mining and Metallurgical Engineers 216, 370-372.
Jung, J.-W., Wan, J., 2012. Supercritical CO2 and ionic strength effects on wettability of silica surfaces: Equilibrium contact angle measurements. Energy & Fuels 26, 6053-6059.
Kozeny, J., 1927. Uber kapillare leitung der wasser in boden. Royal Academy of Science, Vienna, Proc. Class I 136, 271-306.
Krevor, S.C., Pini, R., Zuo, L., Benson, S.M., 2012. Relative permeability and trapping of CO2 and water in sandstone rocks at reservoir conditions. Water Resources Research 48.
Kyte, J., Stanclift Jr, R., Stephan Jr, S., Rapoport, L., 1956. Mechanism of water flooding in the presence of free gas.
Lenormand, R., Touboul, E., Zarcone, C., 1988. Numerical models and experiments on immiscible displacements in porous media. Journal of Fluid Mechanics 189, 165-187.
Li, S., Dong, M., Li, Z., Huang, S., Qing, H., Nickel, E., 2005. Gas breakthrough pressure for hydrocarbon reservoir seal rocks: implications for the security of long-term CO2 storage in the Weyburn field. Geofluids 5, 326-334.
Li, X., Boek, E., Maitland, G.C., Trusler, J.M., 2012. Interfacial Tension of (Brines+ CO2):(0.864 NaCl+ 0.136 KCl) at Temperatures between (298 and 448) K, Pressures between (2 and 50) MPa, and Total Molalities of (1 to 5) mol· kg–1. Journal of Chemical & Engineering Data 57, 1078-1088.
Li, X., Fan, X., 2015. Effect of CO2 phase on contact angle in oil-wet and water-wet pores. International Journal of Greenhouse Gas Control 36, 106-113.
Liang, H.S., Lee, C.H., Wang, J.W., Huang, C.L., Lin, S.L., Huang, T.K., Wu, W.Z., Chen, T.L., 2016. Acquisition and analysis of transient data through unsteady-state core flooding experiments. Journal of Petroleum Exploration and Production Technology 7, 55-68.
Liu, R., Liu, H., Li, X., Wang, J., Pang, C., 2010. Calculation of oil and water relative permeability for extra low permeability reservoir, International Oil and Gas Conference and Exhibition in China. Society of Petroleum Engineers.
Narayanan, N., Mohanadhas, B., Mangottiri, V., 2018. Flow and Transport in Subsurface Environment. Springer.
Nobakht, M., Moghadarn, S., Go, Y., 2007. Effects of viscous and capillary forces on CO2 enhanced oil recovery under reservoir conditions. Energy & Fuels 21, 3469-3476.
Parvazdavani, M., Abbasi, S., Zare-Reisabadi, M., 2017. Experimental study of gas–oil relative permeability curves at immiscible/near miscible gas injection in highly naturally fractured reservoir. Egyptian Journal of Petroleum 26, 171-180.

Perrin, J.-C., Benson, S., 2010. An experimental study on the influence of sub-core scale heterogeneities on CO2 distribution in reservoir rocks. Transport in Porous Media 82, 93-109.
Perrin, J.-C., Krause, M., Kuo, C.-W., Miljkovic, L., Charoba, E., Benson, S.M., 2009. Core-scale experimental study of relative permeability properties of CO2 and brine in reservoir rocks. Energy Procedia 1, 3515-3522.
Primkulov, B.K., Pahlavan, A.A., Fu, X., Zhao, B., MacMinn, C.W., Juanes, R., 2019. Signatures of fluid-fluid displacement in porous media: wettability, patterns, and pressures. arXiv preprint arXiv:1906.02364.
Ramakrishnan, T., Chugunov, N., 2013. Compressibility corrections to relative permeability from the non-uniform steady-state method. Chemical Engineering Science 95, 73-77.
Rapoport, L., Leas, W., 1953. Properties of linear waterfloods. Journal of Petroleum Technology 5, 139-148.
Riazi, M., Sohrabi, M., Bernstone, C., Jamiolahmady, M., Ireland, S., 2011. Visualisation of mechanisms involved in CO2 injection and storage in hydrocarbon reservoirsand water-bearing aquifers. Chemical Engineering Research and Design 89, 1827-1840.
Safi, R., Agarwal, R.K., Banerjee, S., 2016. Numerical simulation and optimization of CO2 utilization for enhanced oil recovery from depleted reservoirs. Chemical Engineering Science 144, 30-38.
Saraji, S., Piri, M., Goual, L., 2014. The effects of SO2 contamination, brine salinity, pressure, and temperature on dynamic contact angles and interfacial tension of supercritical CO2/brine/quartz systems. International Journal of Greenhouse Gas Control 28, 147-155.
Sarmadivaleh, M., Al-Yaseri, A.Z., Iglauer, S., 2015. Influence of temperature and pressure on quartz–water–CO2 contact angle and CO2–water interfacial tension. Journal of Colloid and Interface Science 441, 59-64.
Shi, J.-Q., Xue, Z., Durucan, S., 2011. Supercritical CO2 core flooding and imbibition in Tako sandstone—Influence of sub-core scale heterogeneity. International Journal of Greenhouse Gas Control 5, 75-87.
Shi, J., Durucan, S., 2005. CO2 storage in deep unminable coal seams. Oil & gas science and technology 60, 547-558.
Shiraki, R., Dunn, T.L., 2000. Experimental study on water–rock interactions during CO2 flooding in the Tensleep Formation, Wyoming, USA. Applied Geochemistry 15, 265-279.
Tokunaga, T.K., Wan, J., Jung, J.-W., Kim, T.W., Kim, Y., Dong, W., 2013. Capillary pressure and saturation relations for supercritical CO2 and brine in sand: High-pressure Pc(Sw) controller/meter measurements and capillary scaling predictions. Water Resources Research 49, 4566-4579.
Toth, J., Bodi, T., Szucs, P., Civan, F., 2001. Direct determination of relative permeability from nonsteady-state constant pressure and rate displacements, SPE Production and Operations Symposium. Society of Petroleum Engineers.
Toth, J., Bodi, T., Szucs, P., Civan, F., 2002. Convenient formulae for determination of relative permeability from unsteady-state fluid displacements in core plugs. Journal of Petroleum Science and Engineering 36, 33-44.
Wang, X., Alvarado, V., 2016. Analysis of capillary pressure and relative permeability hysteresis under low-salinity waterflooding conditions. Fuel 180, 228-243.

Xu, R., Luo, S., Jiang, P., 2011. Pore scale numerical simulation of supercritical CO2 injecting into porous media containing water. Energy Procedia 4, 4418-4424.

***Declaration of Interest Statement**

Declaration of interests

☒ The authors declare that they have no known competing financial interests or personal relationships that could have appeared to influence the work reported in this paper.

☐The authors declare the following financial interests/personal relationships which may be considered as potential competing interests: